Fabrication and characterisation of ZrSi$_2$ ceramics via reactive hot-pressing

Yasith C Jayakody, Karthikeyan Ramachandran and Doni Daniel Jayaseelan*

Department of Aerospace and Aircraft Engineering, Kingston University

Roehampton Vale Campus, Friars Avenue, London, United Kingdom, SW15 3DW.

Abstract

ZrSi$_2$ was fabricated via reactive hot-pressing technique for 45 min at 1250°C and 1350°C respectively. The hot-pressed sample exhibited Vickers hardness of 10.93±0.32 GPa and indentation fracture toughness of 3.16±0.54 MPa.m$^{1/2}$. Thermal conductivity (RT-2.99 W/m.K) and diffusivity (RT–18.2 mm^2/s) of sample decreased with increasing temperature due to phonon scattering. Oxidation studies were carried out for the hot-pressed samples from 1000°C to 1200°C for 5, 48 and 100 h in air. The oxidation test results showed that ZrSi$_2$ followed selective oxidation with Si diffusing into the oxide layers at high temperatures. At 1200°C, the surface of ZrSi$_2$ oxidised completely to form a high temperature stable phase, zircon (ZrSiO$_4$). The autoclave test at 250°C and 250 Bar shown negligible mass gain (~0.022g) which suggests the usage of ZrSi$_2$ for nuclear fuel cladding applications.

Keywords: ZrSi$_2$, Oxidation, Fracture toughness, Thermal properties and Autoclave Test.

*Corresponding Author: Dr Doni Daniel Jayaseelan

Email: d.daniel@kingston.ac.uk

Introduction

Zirconium based alloys have been key materials of research in light water based nuclear reactors as fuel cladding materials owing to their excellent corrosion resistance, high mechanical properties, and neutron transparency [1]. However, the structural integrity of the fuel cladding is crucial under various operating conditions such as reactivity-initiated accident (RIA) and loss of coolant accidents (LOCA). Under LOCA environment, the cladding material experiences high oxidation and rapid thermal shock which results in flooding of coolant into reactor core leading to high catastrophe events such as Fukushima Daiichi, Japan [2]. Zirconium based alloys (Zircaloy-4) have been widely used as fuel cladding material. However, the degradation in mechanical properties at high temperatures, oxide spallation, oxidation of material in presence of steam necessitated the search for new fuel cladding material [1]. Following the Fukushima Daiichi, Japan disaster in 2011, the search for high temperature nuclear fuel cladding material has drastically increased with various concepts such as coating the zirconium alloy with high temperature oxidation resistant layer with high accident tolerance and neutron transparency [3, 4].

Previous study reported that coating Zircaloy-4 with Cr resulted in enhanced oxidation resistance but diffusion of O_2 to Zr substrate was observed at high temperature [5]. Oxidation resistant intermetallic coatings such as FeCrAl, Cr_3C_2 and NiCr have been previously studied for their oxidation behaviour in which Cr performed better than other materials. However, Wang *et al.* indicated that FeCrAl was only able to withstand temperature in the range of 700°C to 1000°C in steam environment [6]. In comparison to metallic alloys, numerous transition metal silicides and MAX phase materials are chosen as suitable protective coatings in nuclear and high temperature applications owing to their high oxidation resistance and strength at high temperatures [7]. During high temperature oxidation tests, transition metal silicides, such as $MoSi_2$ and $TiSi_2$ form protective silica which leads to increased oxidation resistance in air. However, in the case of $MoSi_2$, formation of SiO_2 and MoO_3 on the surfaces lead to surface cracks, which disintegrate into powders which are unstable causing pest oxidation [8, 9].

Recently, zirconium-based silicide ($ZrSi_2$) has been under investigation as coating material in nuclear fuel cladding applications due to its lower neutron absorption which is critical in nuclear applications and high strength at elevated temperatures better than other silicides and alloys [10, 11]. Excellent structural and electrical properties of $ZrSi_2$ could be brought out by rapid thermal processing which has made to its utilisation in semiconductor materials with the inclusion of other impurities such as Cu [12]. Most importantly, $ZrSi_2$ has been a key candidate

for the barrier coatings applications owing to formation of its resistive passivation layer ZrO_2 which could protect the substrates during hot corrosion environment [13]. The oxidation of $ZrSi_2$ at 700°C revealed amorphous phases of Zr-Si-O with presence of silicon rich oxide layers. Whereas, at temperature of 1000°C and 1200°C, pure silica phase was found along with isometric layers of ZrO_2 and SiO_2 which were responsible for the oxidation resistance of the $ZrSi_2$ [14]. Yang *et al.* prepared SiC/Si–$ZrSi_2$–ZrB_2-HfB_2/SiC coating through CVD method for C/C composites which shown promising characteristics of self-healing layers [15]. Although, there have been constant research on use of $ZrSi_2$ for barrier coatings and nuclear cladding owing to its superiority towards other Zr-based alloys, studies on the oxide formation of $ZrSi_2$ and its thermal behaviour are not being actively pursued.

In this work, the oxidation studies of reactively sintered $ZrSi_2$ were carried out at high temperatures. Furthermore, thermal and mechanical properties of the reactively sintered $ZrSi_2$ were evaluated.

Materials and Methods

Commercially available zirconium hydride (ZrH_2) with metallic impurities upto 0.3 wt.% (Fishers Scientific Ltd, UK) and silicon (Si) metal powder with impurities upto 0.5 wt.% (Fishers Scientific Ltd, UK) were used as starting materials for the synthesis of $ZrSi_2$. Being highly reactive towards oxygen, the powder processing of ZrH_2 and Si powders was carried out inside a glove box to avoid any surface oxidation and reaction. The glove box was maintained in a controlled atmosphere using argon and oxygen level being maintained at 3ppm. The powders were mixed in stoichiometric ratio using the equation (1).

$$ZrH_2(s) + 2Si(s) \rightarrow ZrSi_2(s) + H_2(g) \tag{1}$$

The powders were dry ball milled using ZrO_2 balls at 150 rpm for 30 min with 5 min of reverse rotation and 10 sec resting in an Argon (Ar) filled container. The milled powder mixture was placed inside a 40 mm graphite die with graphite punches on both sides and kept inside the hot press for sintering. Vacuum hot pressing (FCT Systeme-A) was carried out at a pressure of 30 MPa to fabricate $ZrSi_2$ samples at two different temperatures, 1250°C and 1350°C with a heating and cooling rate of 10°C/min. The thermal profile of vacuum hot pressing is provided in Fig. 1. The samples geometry was 10 mm height and was cut to a diameter of 30mm after sintering to have a total surface area of 1649.33mm^2. The fabricated samples were grounded,

and mirror polished down to 1 μm finish. The $ZrSi_2$ samples fabricated at 1250°C and 1350°C are labelled as S1 and S2, respectively hereafter throughout the text.

Oxidation studies were carried out in the temperature range of 1000°C to 1200°C and for a period of 5, 48 and 100 hrs. The samples were characterised by X-Ray diffraction (XRD) using Bruker-AXS instrument, model D8, with Cu-K alpha radiation (wavelength = 0.1542 nm), Energy-dispersive X-ray spectroscopy (EDS) and scanning electron microscopy (SEM) using Zeiss EVO 50 SEM with associated Oxford Instruments INCA analytical suite techniques before and after oxidation. XRD was carried out at room temperature with 2θ values ranging from 0 to 90° with step of 0.2 sec^{-1}. SEM and EDS analyses were performed on the surface of Au/Pd coated $ZrSi_2$. Vickers hardness was measured for the sintered sample using Zwick/Roell Indented ZHV with help of diamond indenter with load of 10 kN and loading duration of 10 s. Indentation fracture toughness was measured with help of Evan Charles equation specified in equation (2) obtained from earlier study where Hv represents the Vickers hardness, c and a represents towards the geometrical parameters of the crack from Vickers indentation [16, 17].

$$K_{IC} \approx 0.203(H_V\sqrt{a})\left(\frac{c}{a}\right)^{-1.5} \qquad (2)$$

The Vickers hardness and fracture toughness were calculated from the average of 5 tests with same loading condition. The sample was also tested in an autoclave condition with the pressure of 250 Bar and 300°C for 24 hours to determine its suitability in nuclear reactors. Thermal conductivity k is evaluated from density ρ, specific heat Cp and thermal diffusivity α according to the following equation (3):

$$k = \rho \times C_p \times \alpha \qquad (3)$$

Specific heat values were mass averaged from the specific heat of individual components. Thermal diffusivity was measured using a laser flash unit (Netzsch LFA 427, Bavaria, Germany) over the temperature range 25°C to1300°C according to ASTM E1461-13 standard at a heating rate of 10°C/min [18]. The samples were coated with a light spray of graphite to prevent any undesirable reflection from the laser beam. Measurements were performed under vacuum and averaged from at least 3 different laser shots. Thermal diffusivity was measured in at least 3 different samples per composition with differences lower than 0.5%. Thermal expansion of $ZrSi_2$ was calculated from linear thermal expansion, which was measured using a dual push rod dilatometer (Netzsch DIL 402 E, Bavaria, Germany) in helium atmosphere from 25°C to 1300°C according to ASTM standard E228 [19]. The linear thermal expansion

was measured for at least three different samples per material with differences lower than 0.3% and measurements were recorded every 30 s at heating and cooling rates of 10°C/min.

Results and Discussion

Effect of Sintering Temperature

Density studies showed that the samples sintered at 1250°C (S1) had a relative density of 97% and the samples sintered at 1350°C (S2) had a relative density of 99% measured using Archimedes technique suggesting that a low temperature formation of $ZrSi_2$ using reactive synthesis process. Figure 2 shows the XRD patterns of samples S1 and S2 after fabrication. From Figures 2(a) and 2(b), it can be confirmed that the reactively sintered samples contain predominantly $ZrSi_2$ peaks and few weak peaks at 29°, 32° and 36° that correspond to ZrSi. Through Rietveld refinement techniques of diffraction patterns the weight of ZrSi was estimated to be $\leq$ 4 wt.% and other impurities as Hf up to 0.5 wt.%, which was similar to the previous report [20]. Results clearly suggests complete reaction between ZrH_2 and Si to form $ZrSi_2$ however since peaks of ZrO_2 and $ZrSi_2$ are similar at certain peaks there is additional need of elemental analysis which can help to distinguish these phases.

Table 1. Elemental Composition of S1 and S2 samples.

Elements	Elemental Composition (at%)							
	Sample S1				Sample S2			
	A	B	C	D	A	B	C	D
C	0	0	0	12.1	0	7.68	0	0
O	3.57	5.34	68.90	71.5	0	8.12	78	73.59
Si	60.75	44.66	0	0	66.08	44.08	0	3.98
Ti	0.32	0	0	0	0	0	0	0
Zr	31.04	46.34	0	28.31	33.92	0	5.21	22.04
Hf	0	0	27.00	0.25	0	3.98	16.79	0.39

The SE images of the surfaces of the samples S1 and S2 are shown in Figure 3. Visibly few different phases are present in both samples. Although samples S1 and S2 showed almost identical phases in XRD, the composition of the elements varied with the sintering temperatures. Elemental analysis was conducted on four different regions (A, B, C, D) on the surfaces of the S1 and S2 samples and are shown in Table 1. Region A in both samples is the major phase and is identified as $ZrSi_2$ phase from the elemental composition in atomic percentage given in Table 1. This is in comparison to XRD analysis. Similarly, the region

labelled 'B' can be inferred as ZrSi from the elemental analysis shown in Table 1 which has the equal amount of Zr and Si, which is also confirmed in XRD. The occurrence of ZrSi (B) is found locally as patches in both samples. The formation of ZrSi might be attributed to Si deficiency around these regions. Samples S1 and S2 had high amount of Hf in the region labelled 'C'. The appearance of Hf could be since Zr and Hf are found together in the mineral ore due to their similar chemical and physical properties and even with advanced extraction and purification techniques, there is a possibility to have the presence of Hf in Zr sample. Table 1 also reveals that the region labelled 'D' corresponds to ZrO_2 phase. However, this has not been picked up in XRD owing to the reason that they are not present in high amount. The presence of oxygen in regions labelled 'D' on the surfaces of S1 and S2 indicates some oxidation on the surface of the powders. This oxidation of the sample with addition of $ZrSi_2$ reinforcements were previously reported by Liu et al., proving that the $ZrSi_2$ underwent pre-oxidation [21]. The elemental analysis and XRD clearly revealed that the $ZrSi_2$ is the major phase in S1 and S2 samples and the presence of other impurities could be due to the 0.3 % metal-based impurities in the starting material ZrH_2. SEM images of the $ZrSi_2$ samples S1 and S2 taken at high magnification are shown in Fig. 4. From SE images, it can be seen that the S1 sample has slightly more voids on the surfaces than S2. The temperature ranges from 1250 to 1350°C is high enough to have created a bond between Zr and Si leading to formation of highly dense sample with reduced porosity. Aerial analysis technique using image processing software (ImageJ) was used to determine the porosity (%) of the samples along with largest void span and results are plotted in Table 2.

Table 2. Calculated Porosity through linear intercept technique.

Samples	Largest void span (μm)	Total void area (μm²)	Porosity (%)
S1	14.824	880.873	2.16
S2	7.955	395.141	0.97

Mechanical Properties

Vickers hardness and indentation fracture toughness of the samples sintered at 1350°C (S2) were determined with a load of 10 kN and loading duration of 10 s. The crack lengths and indentation lengths were measured with help of SE imagery and respective indentation fracture toughness was calculated through Evan Charles equation from Eq.2 [22]. The average Vickers hardness of the $ZrSi_2$ sample was 10.93 ± 0.32 GPa and fracture toughness was measured to be 3.16 ± 0.54 MPa.m$^{1/2}$ as shown in Table 3. Since the S2 samples had porosity less than 1% than S1 samples, the sample exhibited higher hardness similar to previously reported values [23, 24]. By observing the cracks formed through Vickers indentation, all corners of the instantiation initiated short cracks with the length of the longest crack reported 38.0μm owing to high hardness and moderate fracture toughness of the $ZrSi_2$ ceramics.

Table 3. Fracture toughness and Vickers hardness values for ZrSi₂ samples

Parameters	Values
Hv	10.89
c/a	1.94 ± 0.21
K$_{IC}$ (MPa.m$^{1/2}$)	3.16 ± 0.55
Vickers hardness (GPa)	10.93 ± 0.32

Autoclave Test

The results of the autoclave test performed on $ZrSi_2$ sample at 250°C and 250 Bar pressure for 24 h are reported in Table 4. The results from the autoclave test indicated that the samples shown a colour change after 24 hrs owing to the formation of oxidised phases on the surface. The oxidation of the $ZrSi_2$ was also confirmed by the slight weight gain in the samples of 0.022 g which could result in the negligible phase changes in the $ZrSi_2$ as the material undergone pre-oxidation even while sintering. The change in water colour could be due to the traces of mineral impurities being removed from the $ZrSi_2$ sample. A negligible change in densities before and after autoclave testing reveals that the material did not undergo major physical or chemical changes in the surface proving its stability under nuclear reactor conditions. The dimensional change of the samples with a reduction in the height (~0.014 mm) and increase in weight which could be attributed towards the formation of the oxide layer on the surface.

Table 4. Autoclave test on ZrSi$_2$ samples.

Conditions	Before Experiment	After Experiment (S2)
Weight (g)	0.434	0.456
Height (mm)	3.67	3.656
Density (g/cm^3)	0.505	0.499
Colour	Grey	Light Grey (closer to white)
Water Colour	Ambient	Slight Yellow

Thermal Behaviour

Thermal diffusivity and conductivity of ZrSi$_2$ samples were plotted in Fig.5. Both thermal conductivity and diffusivity showed a reduction in values with increase in temperature. The thermal conductivity of ZrSi$_2$ at room temperature was 3 ± 0.2 W/m.K which dropped by 50% to 1.49 ± 0.4 W/m.K as the temperature increased to1300°C, similarly the diffusivity of the ZrSi$_2$ also showed a reduction from 18.5 mm^2/s to 11 mm^2/s for 1300°C. A plateau at 600°C could be identified beyond which the thermal diffusivity of the sample kept constant up to 1300°C, this might be due to the formation of protective oxide layer which inhibited the thermal transfer from the surface of the samples. Further with increase in temperature, the ZrSi$_2$ formed an oxide layers of ZrO$_2$ on the surfaces of the sample underwent which generally have lower thermal conductivity of 2 W/m.K [25]. The formation of ZrO$_2$ on the surfaces of ZrSi$_2$ samples at high temperature could lead to intrinsic reduction in thermal conductivity due to the scattering of the phonons by point defects by hopping through the oxygen vacancies [25]. From RT to 600°C, the ZrSi$_2$ sample tends to undergo negligible oxidation. However, after 600°C the sample may undergo oxidation rapidly formed a ZiO$_2$ oxide layer along with ZrSiO$_4$ formation at 1200°C which inhibit the diffusivity.

Thermal expansion of the ZrSi$_2$ sample was also studied between room temperature and 1300°C. The average coefficient of thermal expansion of the samples was determined to be 5.2 × 10^{-6} K. The CTE of the samples was highly temperature dependent. The thermal expansion results of the material showed an anomaly behaviour in the temperature range between 0 to 200°C but after 200°C there was a constant increase in the thermal expansion until 1000°C. This could have been due to the negligible formation of oxide layers which resulted in weight gain of the material. Therefore, it can be inferred that the material oxidises at a lower temperature. After 1000°C, there is a plateau observed on the expansion coefficient owing to the selective oxidation of Zr on the surfaces exposed to atmosphere. On the other hand, after

1200°C the formation of $ZrSiO_4$ led to a constant expansion value owing to the high stability of the phase formed. The reduction in the density could be due to the formation of oxides and voids that can alter the thermal expansion resulting in the productions of localised stresses and cracks in the preventive oxidation layer (bimetallic effect) [26]. For coating application, the thermal expansion between the substate and top layer should be closer to avoid thermal mismatch which could lead to cracks between the adhesion layers of the coatings [27, 28]. SiC/SiC CMCs which are preferred for the turbine blades and other hot components have a CTE of ~4.5 × 10^{-6} K [29, 30, 31]. The average CTE of the $ZrSi_2$ (5.2 × 10^{-6} K) was determined to have a closer CTE value as that of SiC/SiC CMCs which makes $ZrSi_2$ an ideal candidate for EBCs [21, 32]. On the other hand, more studies like water vapour corrosion, CMAS corrosion, thermo-mechanical properties, etc are required to understand the effect of $ZrSi_2$ as a EBCs coatings.

Oxidation studies

Oxidation studies were carried out at different temperatures for S2 samples. Figure 6 shows the weight gain rate (g/min) for the $ZrSi_2$ samples as a function of temperature. From Fig. 6, it can be observed that there is no or negligible weight gain up to 1200°C for 5 h owing to good oxidation resistance of the material. This might be due to the formation of ZrO_2 protective layer on the surfaces which initiates to form at 1000°C and its peak were confirmed in the XRD analysis which is detailed further. The behaviour of the sample is the same even when the holding time was increased to 48h. The values clearly show a negligible weight gain at 1200°C for 48 h in comparison with 5h at the same temperature. However, when holding time was increased to 100 h at temperature 1200°C, the rate of weight gain significantly increased to a value of 5.56×10^{-5} g min^{-1} which links to 0.20×10^{-4} g mm^{-2} corresponding to a weight gain when normalised to its surface area of 1649.33 mm^2 whereas in comparison the rate of weight gain of 2.8 ×10^{-5} g min^{-1} (1.56×10^{-5} g mm^{-2}) was recorded in samples incubated for 48h at the same temperature. Figure 7 (a, b and c) shows the XRD patterns of the surfaces after 5 h of oxidation at temperatures 1000°C, 1100°C and 1200°C, respectively as shown in equation (4). However, the presence of $ZrSi_2$ could not be seen at the prolonged duration of time, i.e., 100 h, which is a result of complete oxidation of $ZrSi_2$. The presence of $ZrSi_2$ for 48 h at 1000°C indicates that the material did not oxidise completely in presence of air which proves the thermal stability of the $ZrSi_2$. The formation of the ZrO_2 as baddeleyite which is a more stable state could be seen in the sample oxidised for 100 h at 1000°C shown in Fig. 7(c).

$$ZrSi_2 \ (s) + \ 3O_2(g) \rightarrow ZrO_2 \ (s) + 2SiO_2(s) \tag{4}$$
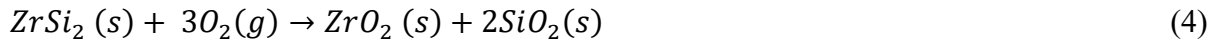
To further understand the weight gain after oxidation, the phase and microstructural analyses were carried out for the oxidised $ZrSi_2$ sample. The SE image shown in Fig. 8 (a and b) and elemental analysis in Table 5 of the $ZrSi_2$ surface after oxidation for 100 h at 1000°C confirm the presence of Zr (10.77%), O (75.05%) and Si (14.19%) elements on the surface of the samples. The presence of high oxygen content from elemental analysis proves the surface oxidation. In samples oxidised for 100 h at 1100°C, SE image shown in Fig.8(c), it can be observed that the sample started to oxidise with formation of ZrO_2 layer and dark spots on the surfaces which was also later determined to be ZrO_2 (baddeleyite). Nodules of Baddeleyite could also be seen in samples oxidised for 1000°C for 100 h as illustrated at Fig. 8(a). From Fig. 8(b), it can be observed that the nodules or unevenness of the ZrO_2 are formed on the surfaces of the samples along with nodules of Baddeleyite which is a result of an internal diffusion that occurred due to selective oxidation of Zr as per the Wanger's theory [33]. This was also observed in the oxidation of $ZrSi_2$ samples at 1100°C. The cross-sectional SE image of the samples oxidised at 1100°C for 100 h (Fig. 8c) evidently shown oxidised layer (light grey) around the sample. The higher concentration of black pigments along with colour change on the surface from grey to darker shade of grey is also clearly seen from the Fig. 8. The change in colour of the samples might be attributed to the diffusion of Si atoms in to oxidised ZrO_2 region due to selective oxidation. According to Wagner theory, the material which is less noble constituent in an alloy or composite could undergo preferential oxidation compared to more noble material [7, 34]. In case of $ZrSi_2$, Si dominates to be a noble element due to presence of stronger covalent bond with its electrons which makes it diffuse into the oxide layers without any reaction with Zr in the Zr-Si system. Being a material with high Si content, the selective oxidation of $ZrSi_2$ leads to formation of Si elements on the surfaces [34]. The diffusion of Si onto the Zr-Si system could be represented in equations (5) and (6) which possibly indicate the formation of two components - Si and SiO_2. The oxidation of $ZrSi_2$ for 48 h and 100 h was pre-dominantly dominated by equations (5) and (6).

$$ZrSi_2 + O_2 \rightarrow ZrO_2 + 2Si \tag{5}$$

$$Si + O_2 \rightarrow SiO_2 \tag{6}$$

The phase analysis and elemental characterisation of the oxidised samples confirm the same with presence of higher baddeleyite peaks on the surfaces with the presence of Zr, O and Si as

reported in the Table 5. XRD pattern in Fig.9(a) did not show up any peaks of Si which were due to the diffusion onto the bulk material which lowered the peaks onto the surfaces but were present in sample oxidised at the sample temperature (1100°C) for 48 h as shown in Fig.9(b) because of cracking due to the formation of the passivation layer exposed the diffused SiO_2. The XRD patterns of the samples oxidised at 1200°C shown in Fig.10(a, b and c) illustrates that the sample oxidised for 5 h consists of three major phases consisting of $ZrSi_2$ and ZrO_2 (both tetragonal and baddeleyite). However, the intensity of the peaks corresponds to both phases of ZrO_2 is relatively small. At 1200°C for 48 h, as shown in Fig.10(b), there is a preferential oxidation of Si present in the samples. The oxidation of the Si to form SiO_2 does not correlate with Deal Grove analysis of Si due to variable in diffusion was not considered prior to oxidation [35]. Domination of the $ZrSi_2$ until the 48 h of oxidation at 1200°C which resulted in increment of composition-scale-factor of 0.106 to 0.953 in crystalline ZrO_2 leading to disappearance of $ZrSi_2$ peaks after the oxidation duration which is evidenced in this Fig. 10. In samples oxidised at 1200°C for 48 h and 100 h, a few peaks in the XRD correspond to $ZrSiO_4$ as obtained in Fig. 10 (b and c). Evidence of the formation of $ZrSiO_4$ could also be seen on the sample oxidised for 100 h at 1100°C but could not be seen for the sample oxidised for 48 h. This infers that the formation of $ZrSiO_4$ is both time and temperature dependant reaction. The lesser peaks for ZrO_2 and SiO_2 as shown in the XRD images shown in Fig10(b and c) is evidence that of the formation of $ZrSiO_4$ consumes ZrO_2 with the diffused SiO_2 which was possibly oxidised following the equation (7):

$$ZrO_2 + SiO_2 \rightarrow ZrSiO_4 \qquad\qquad\qquad (7)$$

Even though SiO_2 has been consumed in the formation of $ZrSiO_4$, SiO_2 has been detected in the XRD patterns of all four samples oxidised at 1100°C and 1200°C for 48 h and 100 h in Fig9(b and c) and Fig10(b and c), respectively. The presence of SiO_2 might be attributed to exposed substrate leading to oxidation, which in turn promotes SiO_2 diffusion. The absence of $ZrSi_2$ in samples oxidised for prolonged hours (100h) in is due to the well-known accelerated oxidation at high temperatures and is evidenced with its presence in all samples for 5h at all temperatures. The formation of $ZrSiO_4$ along with SiO_2 and ZrO_2 was observed at 1100°C for 100 h from phase analysis, and it was found that the composition-scale-factor of the SiO_2 decreased with temperature showing that the oxide phases of Zr reacted with the SiO_2 forming a highly stable $ZrSiO_4$. The formation of $ZrSiO_4$ in sample at 1200°C for 48 itself and enhances its high temperature stability as the material does not undergo any structural transformation

[36]. Contrarily with oxidation there is a possibility of forming cracks on the material also exposes both diffused Si and unreacted $ZrSi_2$ which permits the selective oxidation following Wagner theory to form baddeleyite (ZrO_2) in adequate time which then reacts with diffused Si leading to formation of $ZrSiO_4$ along with other components and hence a steep increment of baddeleyite and the decrement of cristobalite-low (SiO_2) from scale factor 0.19 to 0.07 is being observed at 48 h and 100 h, respectively. With further increase in duration of oxidation time, the peaks corresponding towards the $ZrSi_2$ vanishes leading to formation of a more stable phases of $ZrSiO_4$ and ZrO_2. The presence of baddeleyite is visible in 1200°C samples, but it is not a dominant peak as amorphous ZrO_2, this is due to inadequate time duration to the undergo morphological change from amorphous to baddeleyite which is studied further in the activation energy. The scale factor of the baddeleyite enhanced from 0.056 to 0.40 with increases in duration showing that the material undergoes phase transformation highly from amorphous to baddeleyite at 1200°C [37].

Table 5. Elemental composition of selected regions in $ZrSi_2$ oxidised at 1000°C / 1100°C.

Composition elements (wt%)	1000°C	1100°C		
	-	Region A	Region B	Region C
Zirconium (Zr)	10.77%	30.86%	14.57%	10.55%
Oxygen (O)	75.05%	6.97%	76.28%	79.44%
Silicon (Si)	14.19%	62.16%	9.15%	10.01%

Oxidation kinetics were analysed using the parabolic power law to determine the values of parabolic rate constant (k) of $ZrSi_2$ and reported in Table 6. In equation (8), ΔW represents the weight change prior and after oxidation, A is the total surface area, k = parabolic rate constant and t = oxidation time.

$$\frac{\Delta W}{A} = \sqrt{k \times t} \tag{8}$$

Fig. 11 represents the logarithmic scale of the parabolic constant as function of temperature. The line plotted for the samples oxidised at 5 h at different intervals suggest that weight is increasing with increase in the temperature and time. This parabolic behaviour at 5 h time suggests the diffusion mechanism of oxidation. It is suggested that the noble material Si diffuses into the bulk materials and there is also a constant inward diffusion of oxygen ions depending on temperature. The sample oxidised for 48 h at 1200°C exhibited higher ln(k) value of -7.594 $mg^2mm^{-4}h^{-1}$ compared to its counterpart 1200°C for 100 h with a ln(k) value of -7.39 $mg^2mm^{-4}h^{-1}$, as shown in Table. 5. This could be due to the formation of the $ZrSiO_4$ at 1200°C

which inhibited the diffusion of oxygen into the ZrSi$_2$. To further understand the formation of the oxides on the surfaces of samples, the activation energy (E) was determined using Arrhenius equation represented in eq. (9) theorised by Svante Arrhenius [38].

$$k = Ae^{\frac{-E_a}{RT}}$$ (9)

In eq. (9), A is the constant, R is the gas constant and T is absolute oxidation temperature. From the slope in Fig. 11 and using Eq. (9), the activation energy was determined and reported in Table 6. It can be stated that the activation energy of the samples increases as a function of temperature. As the molecules moves faster owing to higher reaction rates where the respective molecules can easily overcome the activation energy. This phenomenon could be observed with the presence ZrSiO$_4$ at higher temperatures owing to the high diffusion of SiO$_2$ that increased with temperature as validated with XRD patterns. The difference of the activation energies of samples exposed to 5 h of oxidation under temperatures 1100°C and 1200°C and samples exposed to 100 h of oxidation under same temperatures are 0.210 MJ mol^{-1} and 0.206 MJ mol^{-1}. This increase in difference between the activation energy as time increases is due to the formation of ZrSiO$_2$ which was dependent on the diffusion of SiO$_2$ governed by Eq (7), where diffusion of also a time dependant reaction. The activation energy decreases after oxidation due to the material becoming to a more stable stage [39]. The reduction in the activation energies of other samples at lower temperatures (exposed to 5 h, 48 h and 100 h at 1000°C) and for samples oxidised at 1100°C at lower times (5 h and 48 h) and 1200°C for 5 h is not diffusion dependant reaction but purely due to the oxidation of substrate that is governed by Eq (6).

Table 6. Oxidation Kinetics of ZrSi2 (S2) as function of temperature and time.

Time (h)	5			48			100		
Temperature (°C)	1000	1100	1200	1000	1100	1200	1000	1100	1200
Weight change-Experimental (mg)	0.51	0.72	1.35	6.81	13.7	21.2	24.5	168.9	330.7
Weight change calculated (mg)	0.4	0.86	1.299	6.62	14.07	20.07	25.8	168.5	333.6
ln(k) ($mg^2mm^{-4}h^{-1}$)	-8.57	-7.04	-5.81	-9.82	-8.31	-7.59	-9.30	-5.55	-7.39
Activation Energy (MJ mol^{-1})	0.178	0.174	0.172	0.199	0.195	0.194	0.213	0.210	0.206

The oxidation kinetics result suggests that the material followed parabolic law until 1200°C. However, the parabolic constant (k) indicated that samples oxidised at 1200°C for 48 h and 100 h displayed closer ln(k) values Samples oxidised at 48 h shown increased ln(k) values indicating higher rate of ZrO2 diffusion with phase transformation at high temperature. The formation of the protective oxide layer is comparatively faster at higher temperatures, this inhibits oxygen reaching the substrate preventing further oxidation. Due to the inadequate time for diffusion below the rapidly formed inhibition layer, a steeper diffusion gradient is formed. Formation of cracks is inevitable due to the eventually occur due to the thermal stresses present where diffusion occurs along with porous void expansion, hence playing a major role in the activation energy. Comparing the samples oxidised at 5 h, activation energy reduced with increasing temperature which denotes that the sample exposed at 1000°C had the highest oxidation resistance followed by samples oxidised at 1100°C and 1200°C which were confirmed by weight gain.

Conclusion

The present study focused on the fabrication of the $ZrSi_2$ through vacuum reactive hot-pressing technique at two different temperatures, 1250°C and 1350°C. The density studies show that temperature of 1250°C was enough to fabricate high dense $ZrSi_2$. The samples had Vickers hardness of 10.93 ± 0.32 GPa and indentation fracture toughness of 3.16 ± 0.54 MPa.m$^{1/2}$. The homogenous short cracks along the edges of the indentation suggested its brittle behaviour. The formation of stable $ZrSiO_4$ phase is the reason for the reduction in the thermal properties of $ZrSi_2$ at high temperatures. Oxidation behaviour of $ZrSi_2$ under atmospheric air shown that the material undergoes rapid oxidation by forming different phases of ZrO_2 as protective layers. $ZrSi_2$ undergoes parabolic law of oxidation with diffusion of the oxygen inward based on Wangers selective oxidation principle Zr undergoes selective oxidation in the Zr-Si system where Zr is less noble material than the Si which undergoes diffusion onto the protective layers. At 1200°C, the parabolic constant of the $ZrSi_2$ reduces owing to the formation of zircon on the surface due to reaction between the SiO_2 and ZrO_2 phases on the surfaces. The autoclave tests reveal stability of the $ZrSi_2$ samples in nuclear reactor condition, furthermore the study evidenced the high properties of $ZrSi_2$ which could lead to future works for considering the material to be studied for future in-depth for nuclear fuel-cladding applications. Coefficient of thermal expansion of the $ZrSi_2$ was closer to 5×10^{-6} K proving that the material could act as possible EBC for SiC/SiC composites owing to its closer CTE match.

References

[1] J. Kim, H. Kim and H. Ryu, "High-temperature oxidation behaviors of $ZrSi_2$ and its coating on the surface of Zircaloy-4 tube by laser 3D printing," *Nuclear Engineering and Technology* , vol. 52, no. 9, pp. 2054-2063, 2020.

[2] H. Kim, J. Kim, J. moon, H. Lee, J. Kim and Y. Chai, "High-temperature Oxidation Behavior of Zircaloy-4 and Zirlo in Steam Ambient," *Journal of Materials Science & Technology* , vol. 26, no. 9, pp. 827-832, 2010.

[3] J. Kim, T. Ha, I. Kim and H. Kim, "Microstructure and Oxidation Behavior of CrAl Laser-Coated Zircaloy-4 Alloy," *Metals* , vol. 7, no. 2, p. 59, 2017.

[4] X. Han, Y. Wang, S. Peng and H. Zhang, "Oxidation behavior of FeCrAl coated Zry-4 under high temperature steam environment," *Corrosion Science* , vol. 149, pp. 45-53, 2019.

[5] D. Jin, F. Yang, Z. Zou, L. Gu, X. Zhao, F. Guo and P. Xiao, "A study of the Zirconium alloy protection by Cr_3C_2–NiCr coating for nuclear reactor application," *Surface and Coatings Technology,* vol. 287, pp. 55-60, 2016.

[6] Y. Wang, H. Tang, X. Han, W. Feng, X. Zhou, S. Peng and H. Zhang, "Oxidation resistance improvement of Zr-4 alloy in 1000°C steam environment using ZrO_2/FeCrAl bilayer coating," *Surface Coating Technology* , vol. 349, pp. 807-815, 2018.

[7] K. Ramachandran, Z. Carmine, K. Yoshida, T. Tsunoura and D. Jayaseelan, "Experimental investigation and mathematical modelling of water vapour corrosion of Ti_3SiC_2 and Ti_2AlC ceramics and their mechanical behaviour," *Journal of the European Ceramic Soceity,* vol. 41, no. 9, pp. 4761-4773, 2021.

[8] C.G.Mckamey, P.F.Tortorelli, J.H.Devan and C.A.Carmichael, "A study of pest oxidation in polycrystalline $MoSi_2$," *Journal of Materials Research* , pp. 2724-2755, 1992.

[9] S.Melsheimer, M.Fietzek, V.Kolarik, A.Rahmel and M.Schutze, "Oxidation of the intermetallics $MoSi_2$ and $TiSi_2$ - a comparison," *Oxidation of Metals* , vol. 47, pp. 139-203, 1997.

[10] Z. Zaki, Q. Mohsen, S. Alotaibi and M. E. Sadek, "Studying the self-healing reaction based on zirconium silicide in the thermal barrier coating system," *Journal of Ceramic Processing Research,* vol. 21, no. 2, pp. 192-199, 2020.

[11] H. Yeom, "High temperature corrosion and heat transfer studies of Zirconium-Silicide coatings for light water reactor cladding applications," Proquest Dissertations Publishing, The university of Wisconsin-Madison , 2017.

[12] M.Setton and J. Spiegel, "Structural and electrical properties of $ZrSi_2$ and Zr_2CuSi_4 formed by rapid thermal processing," *Journal of Applied Physics* , vol. 70, no. 1, 1998.

[13] M.Parchoviansky, G. Barroso, I.Petrikova and G.Motz, "Polymer derived glasss ceramic layers for corrosion protection of metals," in *Advanced and Refractory Ceramics for Energy Conservation and Efficiency*, The American Ceramic Society, pp. 187-196.

[14] H. Yeom, B. Maier, R. Mariani, D. Bai and K. Sridharan, "Evolution of multilayered scale structures during high temperature oxidation of $ZrSi_2$," *Journal of Material Research*, vol. 31, pp. 3409-3419, 2016.

[15] X. Yang, H. Quan and K. Wang, "SiC/Si–$ZrSi_2$–ZrB_2-HfB_2/SiC coating for oxidation protection of C/C composites prepared by three-step method," *Journal of Alloys and Compounds,* vol. 836, no. 155532, 2020.

[16] T. Arunkumar, G. Anand, R. Subbiah, R. Karthikeyan and J. Jeevahan, "Effect of multiwalled carbon nanotubes on improvement of fracture toughness of spark-plasma-sintered Yttria-stabilized zirconia nanocomposites," *Journal of Materials Engineering and Performance,* vol. 30, pp. 3925-3933, 2021.

[17] K. Ramachandran, V. Boopalan, J. Bear and R. Subramani, "Multi-walled carbon nanotubes (MWCNTs) - reinforced ceramic nanocomposites for aerospace applications: a review," *Journal of Materials Science,* vol. 57, pp. 3923-3953, 2022.

[18] ASTM. E1461-13, "Standard Test Method for Thermal Diffusivity by the Flash Method," ASTM, USA.

[19] ASTM. E228-95, "Standard Test Method for Linear Thermal Expansion of Solid Materials With a Vitreous Silica Dilatometer," ASTM International, West Conshohocken, PA, 2005.

[20] H. GeBwein, A. Pfrengle, J. Binder and J. Haubelt, "Kinetic model of oxidation of $ZrSi_2$ powders," *Journal of Thermal Analysis and Calorimetry,* vol. 91, no. 2, pp. 517-523, 2008.

[21] F. Liu, H. Li, S. Gu, X. Yao and Q. Fu, "Spraying power influence on microstructure and bonding strength of $ZrSi_2$ coating for SiC coated carbon/carbon composites," *Ceramics International*, vol. 44, no. 6, pp. 6619-6626, 2018.

[22] K. Liang, G. Orange and G. Fantozzi, "Evaluation by indentation of fracture toughness of ceramic materials," *Journal of Materials Science*, vol. 25, pp. 207-214, 1990.

[23] M. Wang, C. Wang and X. Zhang, "Effects of SiC platelet and $ZrSi_2$ additive on sintering and mechanical properties of ZrB2-based ceramics by hot-pressing," *materials and Desgin*, vol. 34, pp. 293-297, 2012.

[24] B. Ma and S. Xu, "Microstructure and mechanical properties of ternary ceramic composites with a ZrC-SiC matrix," *Journal of Ceramic Science and Technology*, vol. 7, no. 4, pp. 335-339, 2016.

[25] K. Sclichting, N. Padture and P. Klemens, "Thermal conductivity of dense and porous yttria-stabilized zirconia," *Journal of Materials Science*, vol. 36, pp. 3003-3010, 2001.

[26] G. Mehboob, M.-J. Liu, T. Xu, S. Hussain, G. Mehboob and A. Tahir, "A review on failure mechanism of thermal barrier coatings and strategies to extend their lifetime," *Ceramics International,* vol. 46, no. 7, pp. 8497-8521, 2020.

[27] N. Nasiri, N. Patra, D. Horlait, D. Jayaseelan and W. Lee, "Thermal properties of rare-earth monosilicates for EBC on Si-based ceramic composites," *Journal of the American Ceramic Society,* vol. 99, no. 2, pp. 589-596, 2016.

[28] S. Ueno, D. Jayaseelan and T. Ohji, "Development of oxide-based EBC for silicon nitride," *International Journal of Applied Ceramic Technology,* vol. 1, no. 4, pp. 362-373, 2004.

[29] N. Nasiri, N. Patra, D. Jayaseelan and W. Lee, "Oxidation behaviour of SiC/SiC ceramic matrix composites in air," *Journal of the European Ceramic Society*, vol. 36, no. 14, pp. 3293-3302, 2016.

[30] K. Lee, D. Fox and N. Bansal, "Rare earth silicate environmental barrier coatings for SiC/SiC composites and Si_3N_4 ceramics," *Journal of the European Ceramic Society*, vol. 25, no. 10, p. 17051715, 2005.

[31] K. Ramachandran, S. Leelavinodhan, C. Antao, A. Copti, C. Mauricio, Y. Jyothi and D. Jayaseelan, "Analysis of failure mechanisms of Oxide - Oxide ceramic matrix composites," *Journal of the European Ceramic Society*, vol. 4, no. 1626-1634, p. 42, 2022.

[32] K. Nakano, N. Fukatsu and Y. Kanno, "Thermodynamics of Zr/Hf-mixed silicates as a potential for environmental barrier coatings for Tyranno-hex materials," *Surface and Coatings Technology*, vol. 203, no. 14, pp. 1997-2002, 2009.

[33] A. Atkinson, "Wagner theory and short circuit diffusion," *Materials Science and Technology*, vol. 4, no. 12, pp. 1046-1051, 2013.

[34] C. Wagner, "Oxidation of alloys involving noble metals," *The Electrochemical Society,* vol. Volume 103, Number 10, 1956.

[35] B. Deal and A. Grove, "General relationship for the thermal oxidation of Silicon," *Jounral of Applied Physics,* vol. 36, no. 12, pp. 3770-3778, 1965.

[36] N. Rendtorff, L. Garrido and E. Aglietti, "Mechanical and fracture properties of zircon–mullite composites obtained by direct sintering," *Ceramics International*, vol. 35, no. 7, pp. 2907-2913, 2009.

[37] L. Gao, Q. Liu, J. Hong, H. Miyamoto, D. Torre, A. Kakitsuji, K. Liddell and D. Thompson, "Phase transformation in the Al_2O_3–ZrO_2 system," *Journal of Materials Science*, pp. 1399-1403, 1998.

[38] M. Peleg, M. D. Normand and M. G. Corradini, "The Arrhenius equation revisited," *PubMed,* 2021.

[39] V. Vettegren, A. Bashkarev, K. Danchukov and G. Morozov, "The kinetics of steel corrosion in sea water," *Technical Physics Letters,* vol. 29, pp. 64-65, 2003.
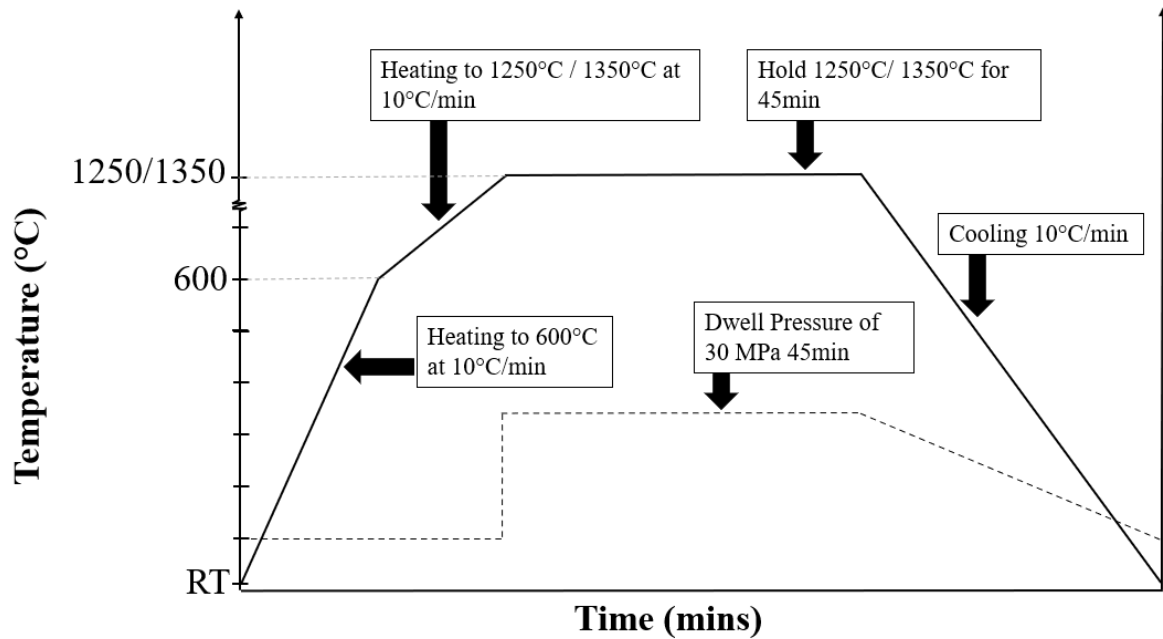
Figure 1. Temperature and pressure profiles for vacuum hot pressing.
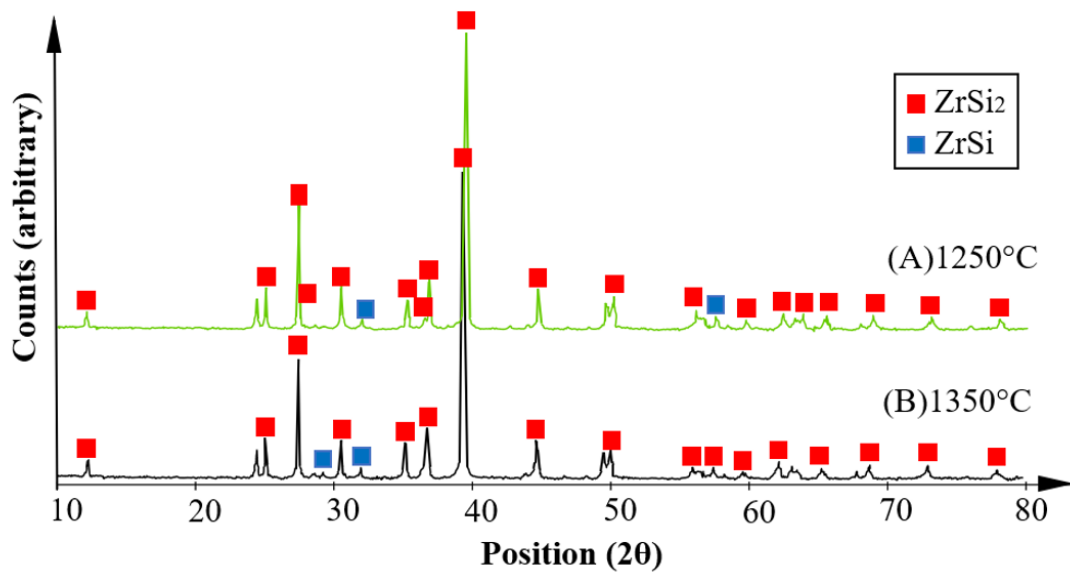
Figure 2. Phase composition of ZrSi₂ sintered at (a) 1250°C and (b) 1350°C
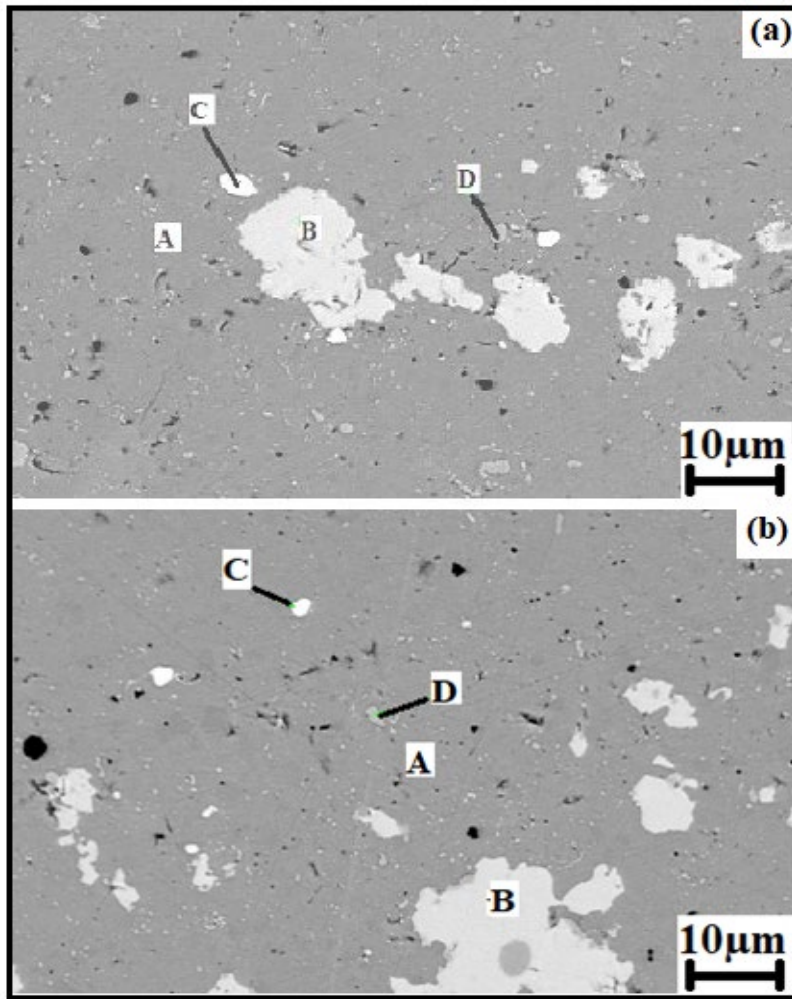
Figure 3. SE image indicating elemental analysis on (a) S1 sample and (b) S2 sample.
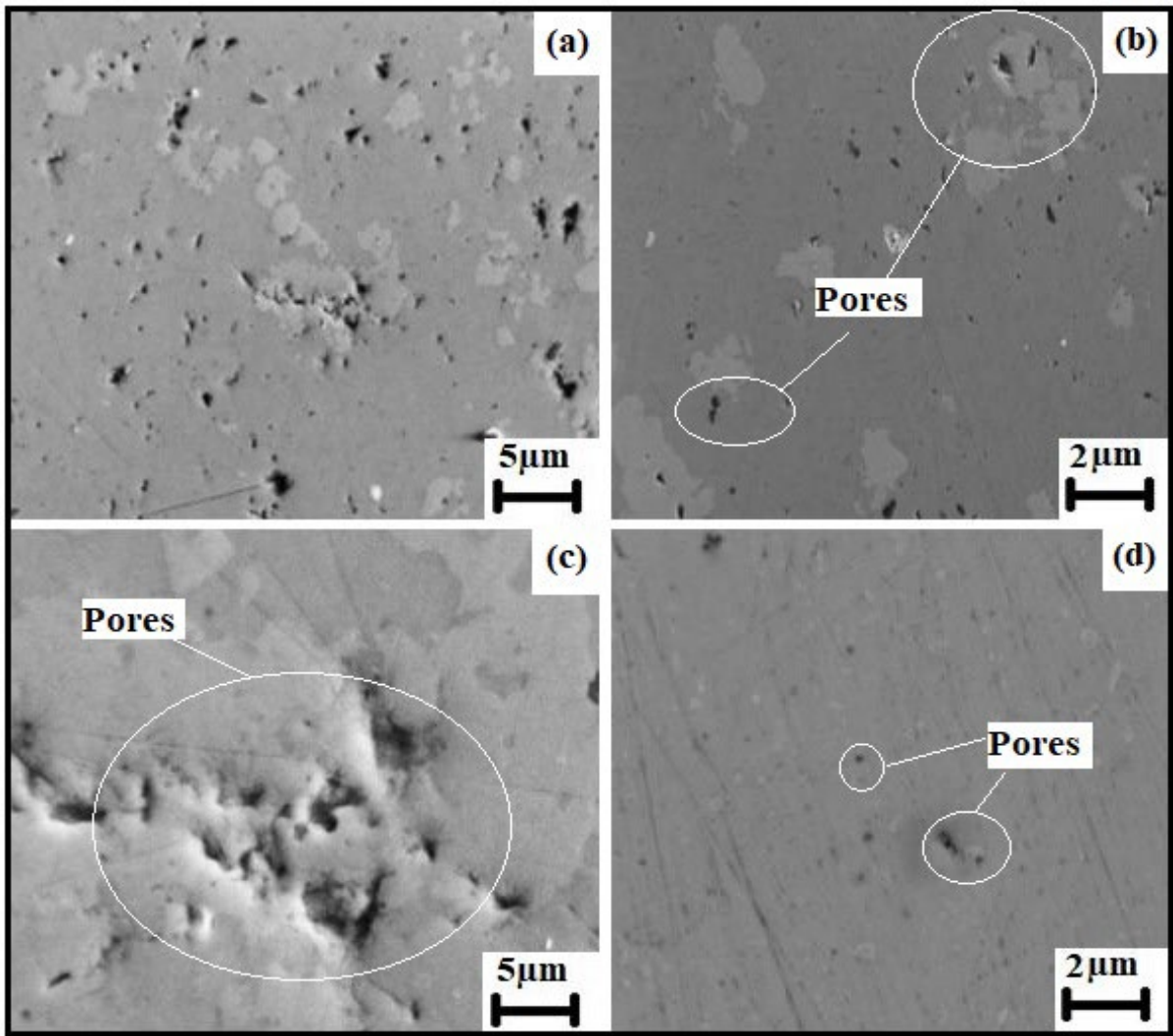
Figure 4. SEM images highlighting pores of ZrSi₂ samples sintered at (a & c) 1250°C, (b & d) 1350°C.
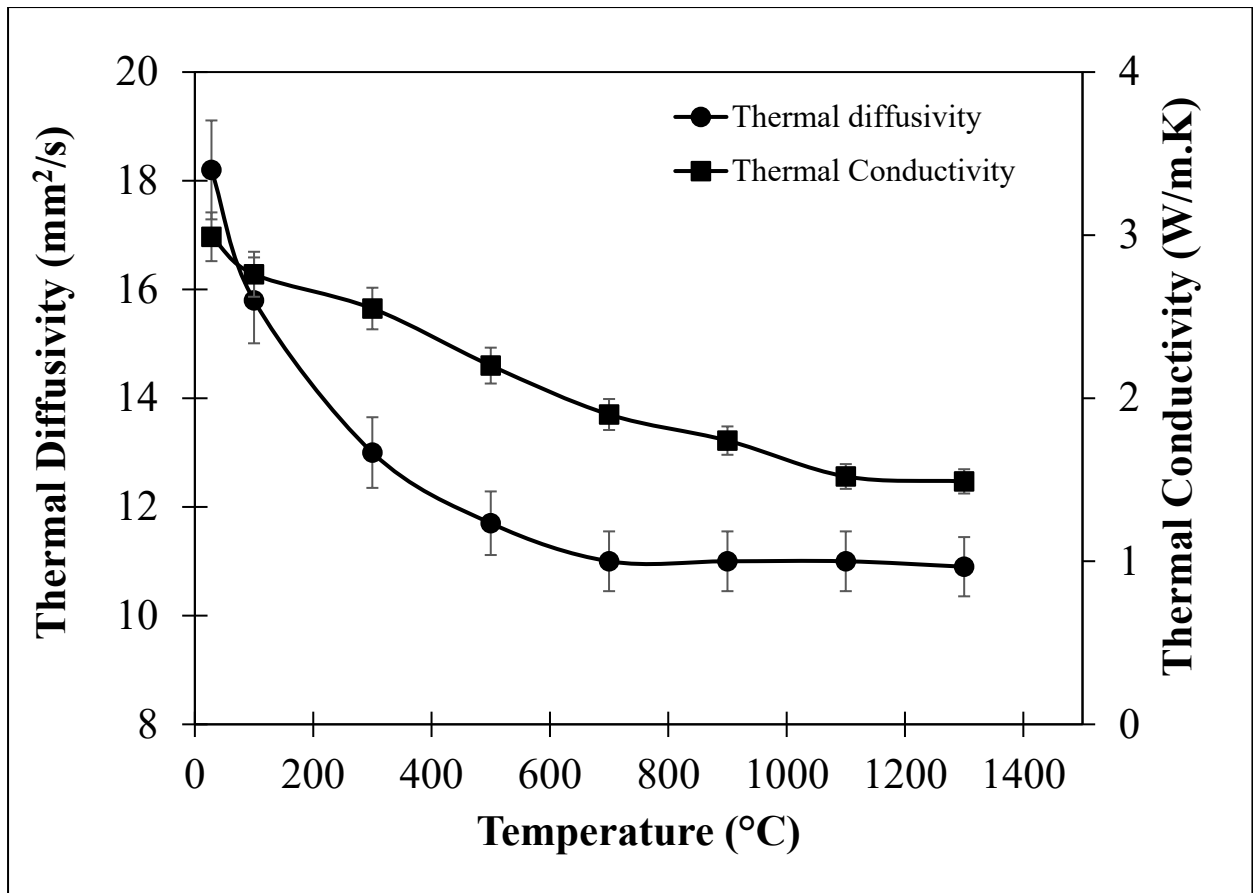
Figure 5. Thermal conductivity and diffusivity of ZrSi$_2$ in sample S2 as function of temperature.
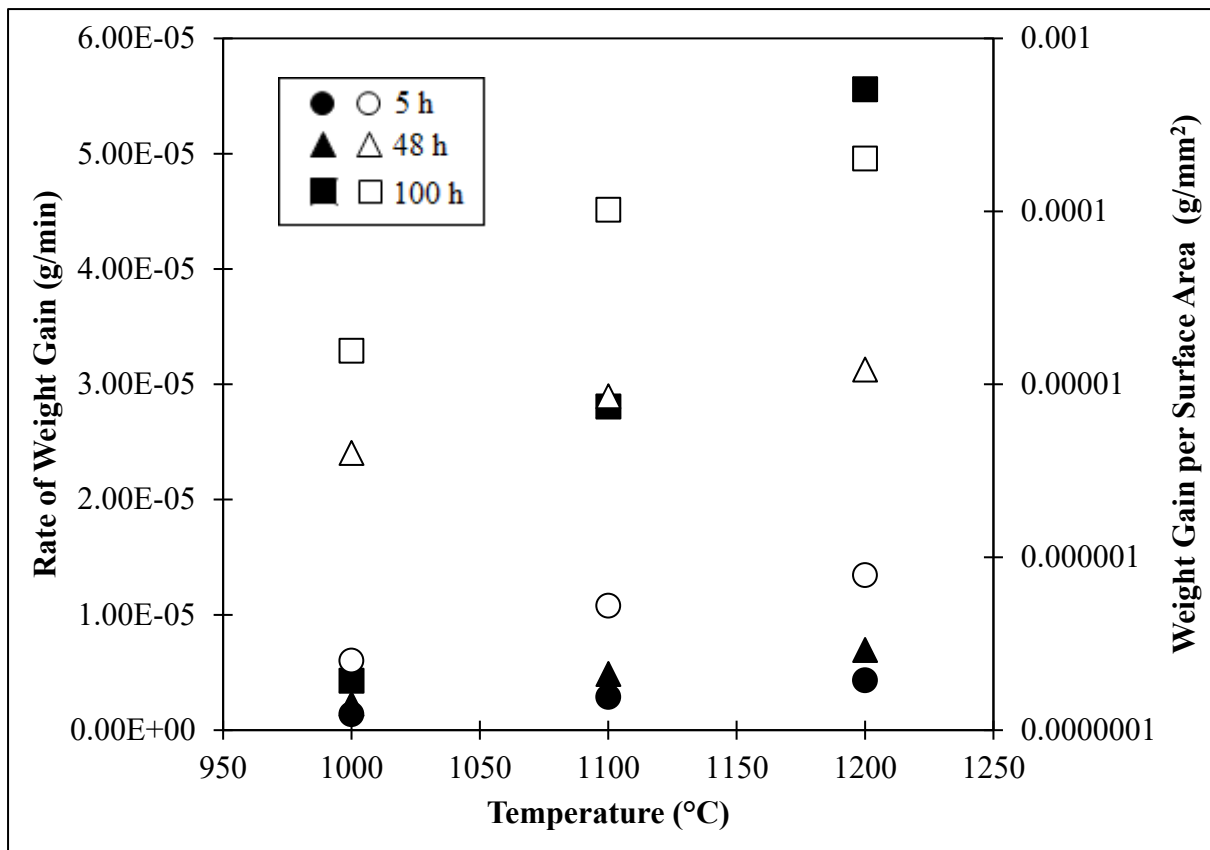
Figure 6. Rate of weight gain plotted as function of temperature with its representation normalised to the surface area during oxidation.
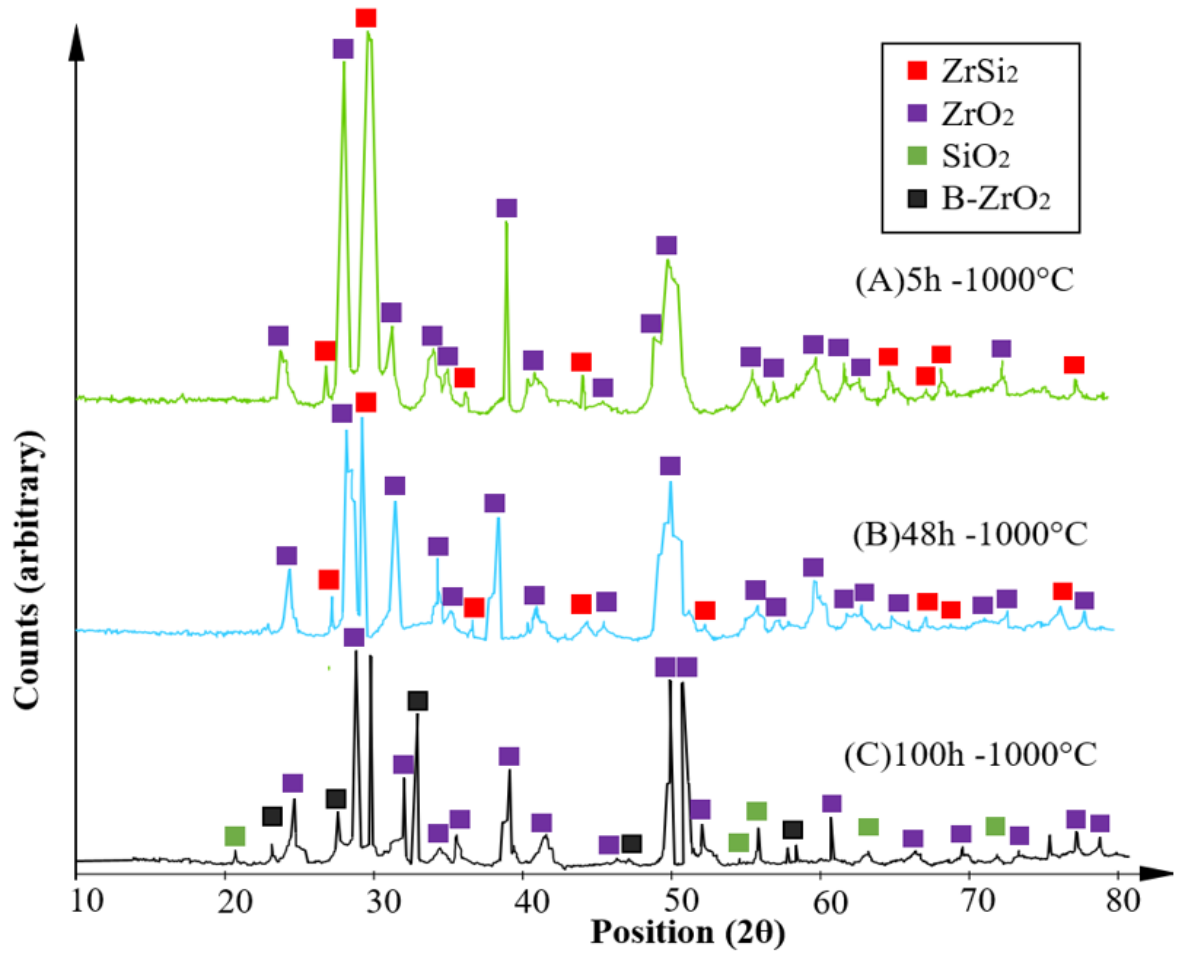
Figure 7. X-Ray diffraction patterns of ZrSi₂ sample oxidised at 1000°C at different time intervals (a) 5 h (b) 48 h and c) 100 h.
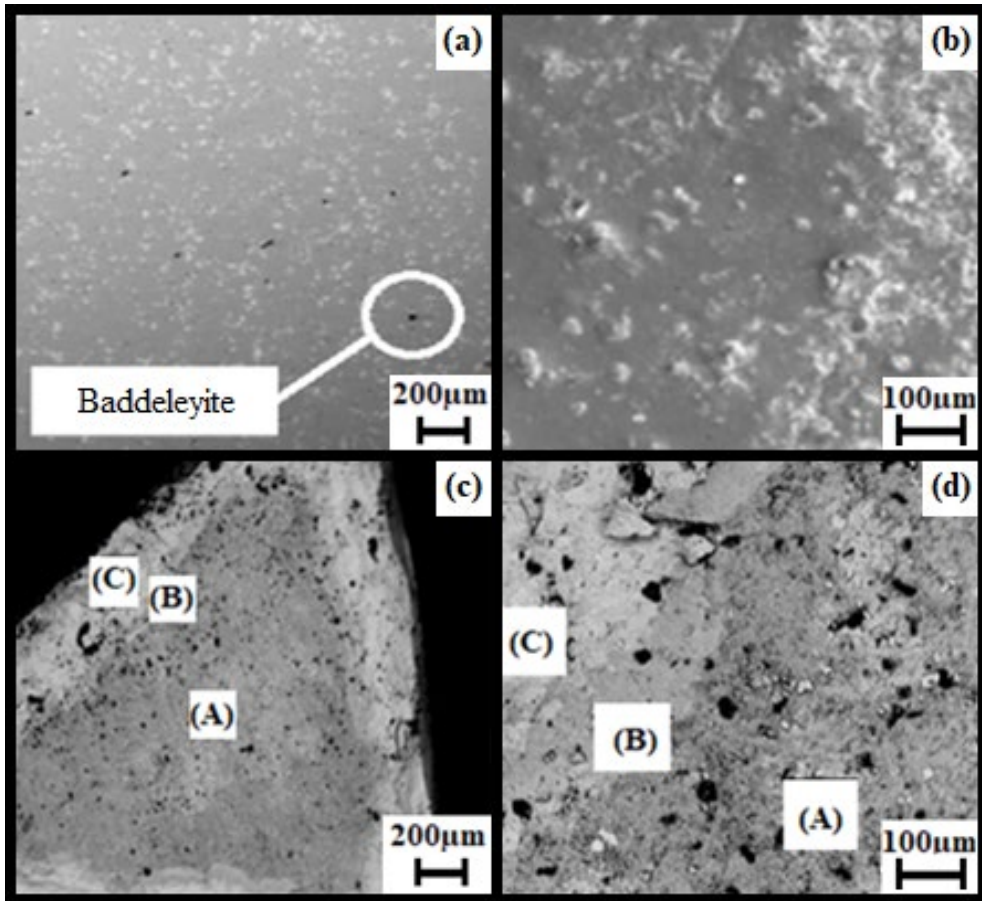
Figure 8. SE image of ZrSi₂ oxidised for 100 h at various oxidisation temperatures (a & b) 1000°C, (c & d) 1100°C
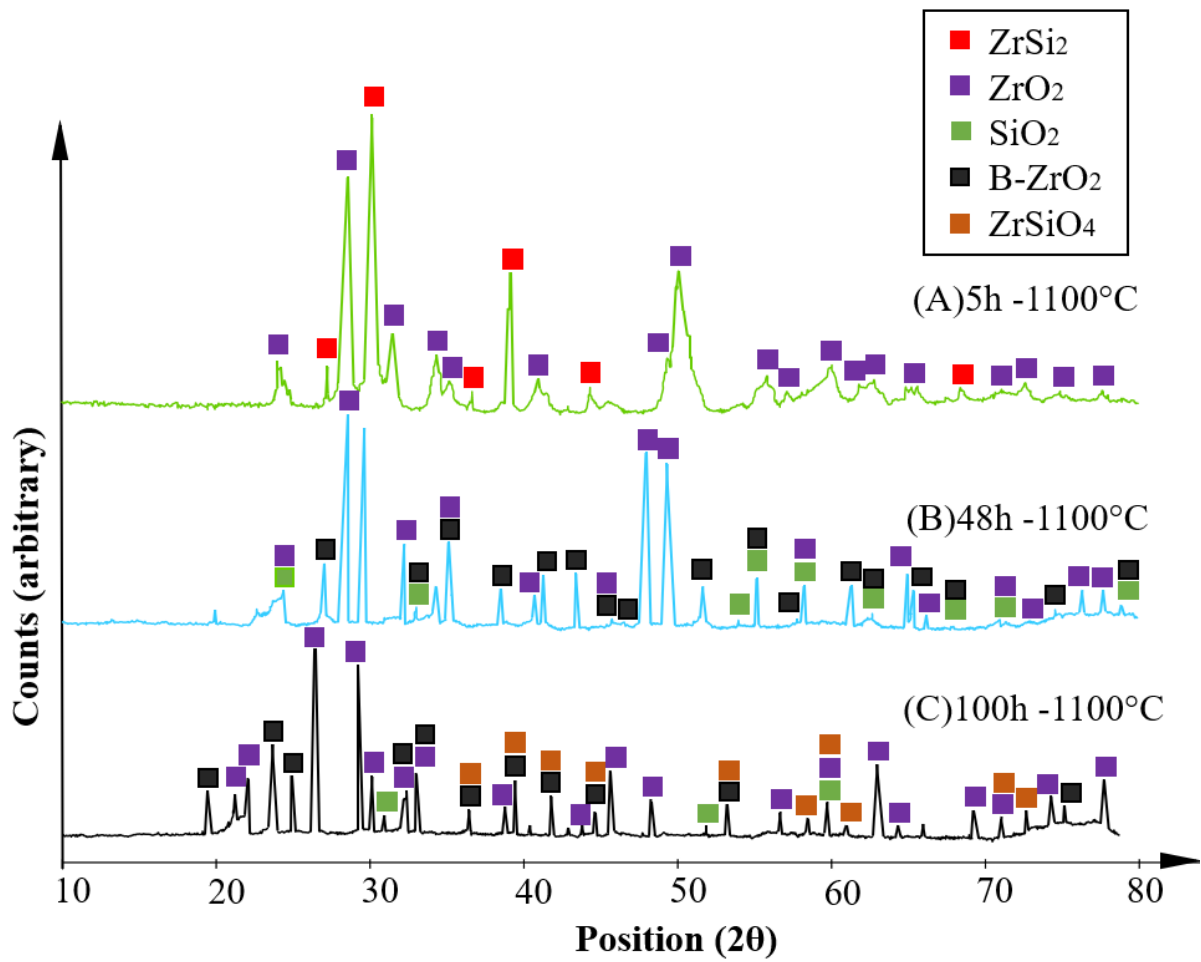
Figure 9. X-Ray diffraction patterns of ZrSi₂ sample oxidised at 1100°C at different time intervals (a) 5 h (b) 48 h and c) 100 h.
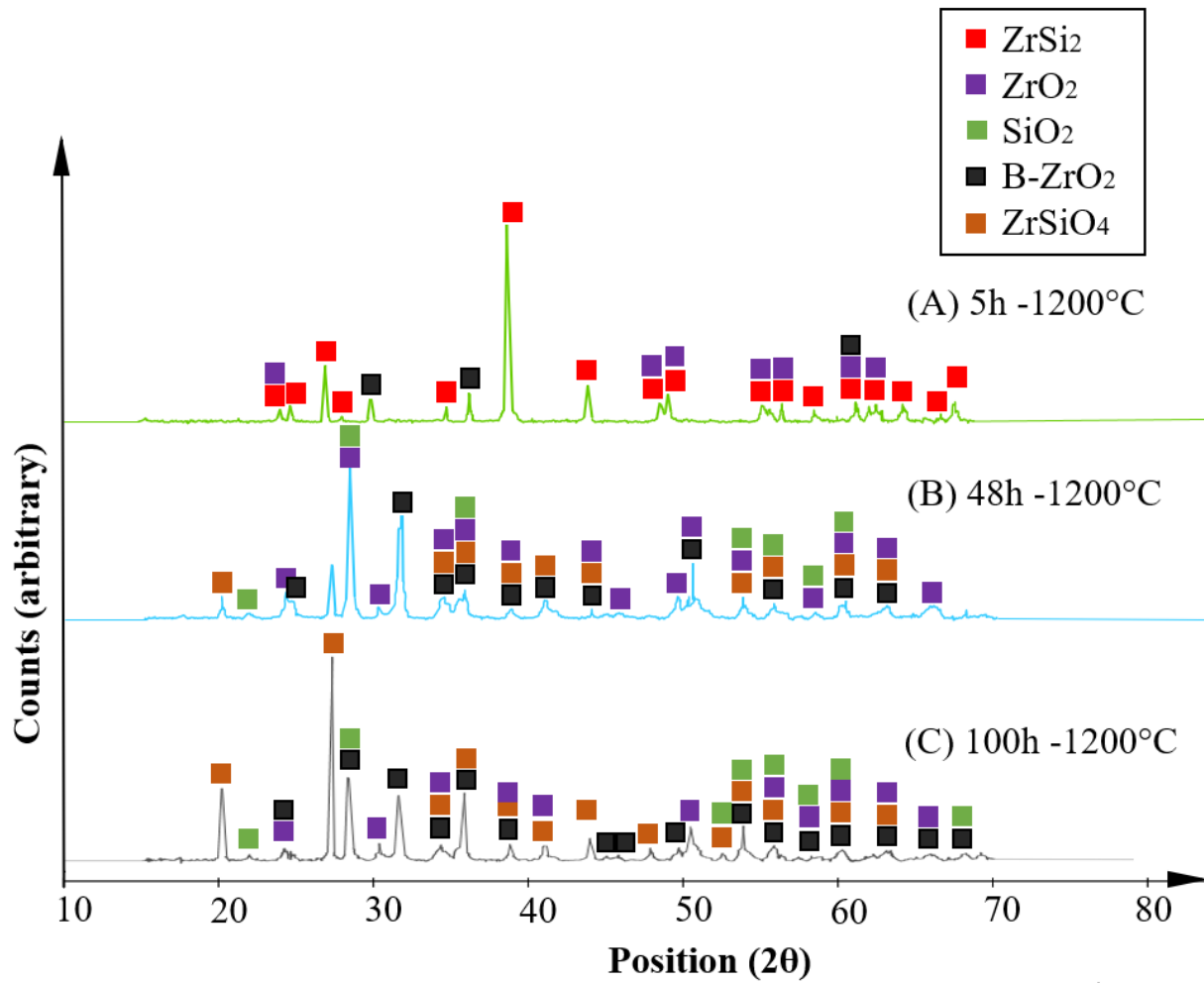
Figure 10. X-Ray diffraction patterns of ZrSi₂ sample oxidised at 1200°C at different time intervals (a) 5 h (b) 48 h and c) 100 h.
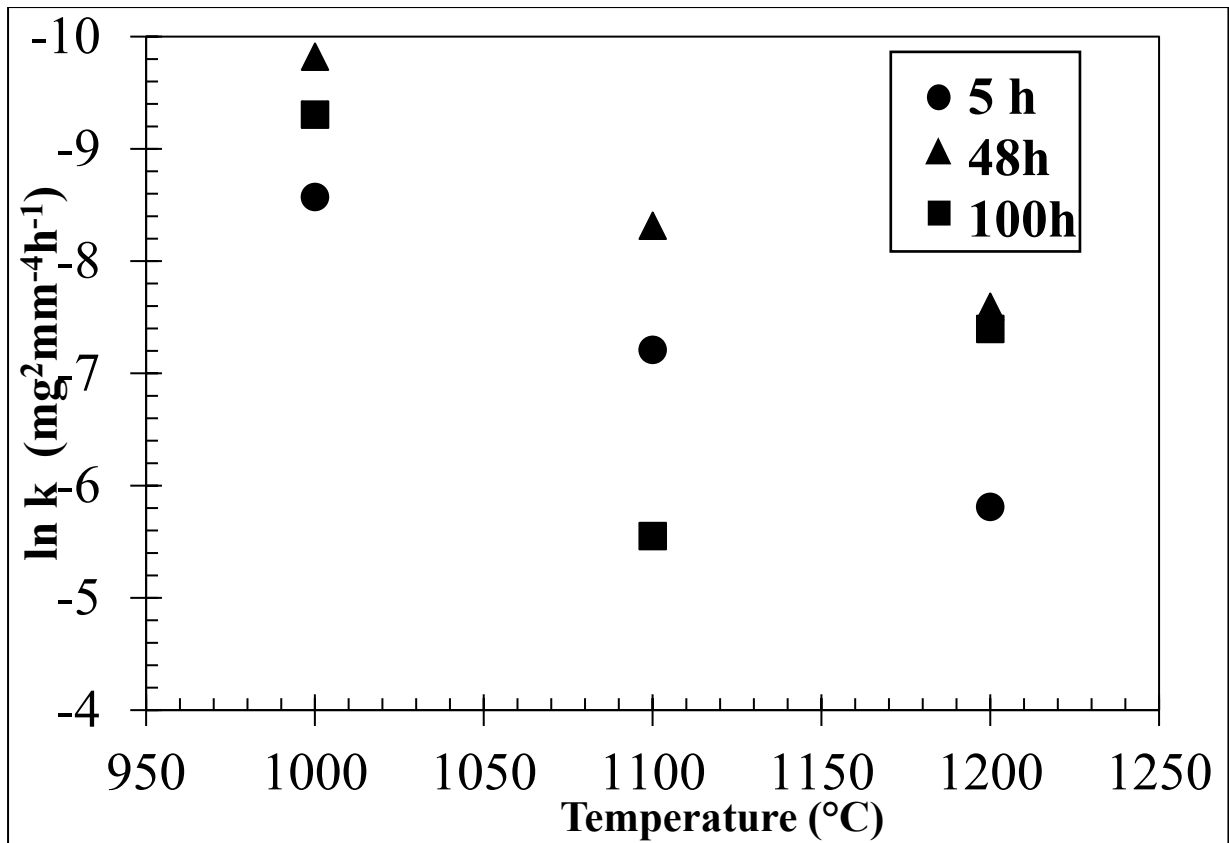
Figure 11. Parabolic rate constant plotted against temperature for ZrSi$_2$ (S2) samples.